PCCP

Accepted Manuscript

This article can be cited before page numbers have been issued, to do this please use: A. S. Cuharuc, G. Zhang and P. R. Unwin, *Phys. Chem. Chem. Phys.*, 2016, DOI: 10.1039/C5CP06325F.

ROYAL SOCIETY OF CHEMISTRY

www.rsc.org/pccp

View Article Online
DOI: 10.1039/C5CP06325F

Journal Name

ARTICLE

Electrochemistry of Ferrocene Derivatives at Highly Oriented Pyrolytic Graphite (HOPG): Quantification and Impact of Surface Adsorption†

Received 00th January 20xx,
Accepted 00th January 20xx

DOI: 10.1039/x0xx00000x

www.rsc.org/

Anatolii S. Cuharuc,[§] Guohui Zhang[§] and Patrick R. Unwin[*]

Cyclic voltammetry of three ferrocene derivatives – (ferrocenylmethyl) trimethylammonium ($FcTMA^+$), ferrocenecarboxylic acid (FcCOOH), and ferrocenemethanol ($FcCH_2OH$) – in aqueous solutions shows that the reduced form of the first two redox species weakly adsorbs on freshly cleaved surfaces of highly oriented pyrolytic graphite (HOPG), with the fractional surface coverage being in excess of 10% of a monolayer at a bulk concentration level of 0.25 mM for both compounds. $FcCH_2OH$ was found to exhibit greater and stronger adsorption (up to a monolayer) for the same bulk concentration. Adsorption of $FcTMA^+$ on freshly cleaved surfaces of high quality (low step edge density) and low grade (high step edge density) HOPG is the same within experimental error, suggesting that the amount of step edges has no influence on the adsorption process. The amount of adsorption of $FcTMA^+$ is the same (within error) for low grade HOPG, irrespective of whether the surface is freshly cleaved or left in air for up to 12 hours, while – with aging – high quality HOPG adsorbs notably more $FcTMA^+$. The formation of an air-borne contaminating film is proposed to be responsible for the enhanced entrapment of $FcTMA^+$ on aged high quality HOPG surfaces, while low quality surfaces appear less prone to the accumulation of such films. The impact of the adsorption of ferrocene derivatives on graphite on voltammetric studies is discussed. Adsorption is quantified by developing a theory and methodology to process cyclic voltammetry data from peak current measurements. The accuracy and applicability, as well as limits of the approach, are demonstrated for various adsorption isotherms.

Introduction

Carbon electrodes, especially graphene, carbon nanotubes and pyrolytic graphite as representatives of the sp^2 carbon family, acquire increasing significance in fundamental and applied electrochemistry.[1] A range of properties, such as the inherent conductivity, biocompatibility, chemical inertness, low background current, capacitance density in solutions and low cost make this family of carbons particularly attractive for applications spanning from biosensors[2–4] and electronics[5] to fuel cell electrodes.[6,7] On the other hand, the high specific surface area of functionalized nanocarbons also make these materials very powerful for electrochemical supercapacitors.[8,9]

Electrochemical reactions of fundamental and practical importance for sp^2 carbon electrodes range from complex muli-step electron-proton coupled reactions (e.g. oxygen reduction,[10,11] and the oxidation of neurotransmitters in aqueous solutions[12,13]), to outer-sphere reactions (e.g. simple one-electron processes,[14–16] and the reduction of diazonium salts[17,18]). Moreover, various benchmark redox systems have been considered as a general means of assessing the electroactivity and quality of carbon electrodes, among which ferrocene derivatives, which are known to undergo fast outer-sphere ET on (noble) metals[19–21] are popular. Examples of the use of ferrocene derivatives are numerous and some of them are briefly discussed herein. (Ferrocenylmethyl) trimethylammonium ($FcTMA^+$) was used to demonstrate the dependence of ET kinetics on the number of layers of chemical vapour deposited (CVD) graphene,[22] to test the redox-dependent electroactivity of graphene[23] and graphite edges,[24] and for characterizing the electrochemistry of networks of single-walled carbon nanotubes (SWNTs).[25–27] Other frequently used derivatives are ferrocenemethanol ($FcCH_2OH$) and ferrocenecarboxylic acid (FcCOOH) that, along with $FcTMA^+$, were employed for ET kinetic studies at SWNTs and multi-walled carbon nanotubes,[28–30] pristine and defected graphene,[31–34] and highly oriented pyrolytic graphite (HOPG).[35–37]

Ferrocene derivatives can also adsorb on carbon electrodes from aqueous solutions, an aspect that is not always appreciated, but needs to be fully understood for the appropriate analysis of voltammetric responses. One of the few studies in this area is from Bond and co-workers[38] who examined the applicability of ferrocene as a standard voltammetric reference in aqueous media. Evidence for weak adsorption was found for all electrode materials tested, in

Department of Chemistry, University of Warwick, Coventry, CV4 7AL, UK.
† Electronic Supplementary Information (ESI) available: [details of any supplementary information available should be included here]. See DOI: 10.1039/x0xx00000x
§ These authors contributed equally.

View Article Online
DOI: 10.1039/C5CP06325F

various supporting electrolytes, with glassy carbon showing the strongest adsorption effect on the voltammetric response for several techniques (cyclic voltammetry, differential pulse voltammetry and normal pulse voltammetry). A small amount of (irreversible) adsorption of $FcCH_2OH$ onto CVD graphene has also been reported,[31] with an estimation of surface coverage of 1.1 x 10^{-11} mol/cm^2 (from a bulk solution of 1 mM of this redox mediator) that constituted ~ 2% of a monolayer. The significance of electrode adsorption (particularly of ferrocene derivatives) has also been recognized in single molecule studies.[39,40]

Here, we present a cyclic voltammetry (CV) study of the electrochemistry of ferrocene derivatives at HOPG, mainly focused on $FcTMA^{2+/+}$ but also including $FcCOO^{-/0}$ and $FcCH_2OH^{+/0}$. We show that the reduced forms of all of these compounds adsorb on the HOPG surface ($FcTMA^+$ ~ $FcCOO^-$ < $FcCH_2OH$), whereas the oxidized forms do not. We extract the surface concentration of adsorbed $FcTMA^+$ quantitatively at different bulk concentrations, based on a simple theoretical model, which can be used to obtain an empirical isotherm in the case of $FcTMA^+$ adsorption at HOPG. Additionally, the adsorption of $FcTMA^+$ on freshly cleaved HOPG was found to be independent of the HOPG quality (step edge density), although differences in the amount of adsorption of HOPG emerge when samples are left to age in air. The significance of accounting for surface adsorption when considering the electrochemistry of ferrocene derivatives in fundamental voltammetric studies is discussed, particularly in light of recent investigations aimed at understanding the electrochemistry of sp^2 carbon electrodes.

Experimental

Materials and chemicals

$FcTMA[PF_6]$ was synthesized in-house via an exchange reaction of $FcTMA^+I^-$ (Strem Chemicals, Ltd.) with $AgPF_6$ (Strem Chemicals, Ltd.).[41] $FcCH_2OH$ (97%) and KCl (99%) were purchased from Sigma-Aldrich, and FcCOOH (98%) was from Alfa Aesar. All were used as received. All solutions were freshly prepared using Millipore Milli-Q water, with a resistivity *ca*. 18.2 MΩ cm at 25 °C.

Sample preparation

SPI-3 grade HOPG was purchased from SPI Supplies (West Chester, PA). An HOPG block of high quality, but ungraded, was kindly provided by Prof. R. L. McCreery (University of Alberta, Canada), originating from Dr. A. Moore, Union Carbide (now GE Advanced Ceramics), and so referred to as AM grade herein. A fresh surface of HOPG was exposed prior to each experiment by peeling off the top layers with Scotch tape as routinely done in the literature,[14–16,42–48] and shown to be equivalent to mechanically cleaved HOPG.[14,15] These HOPG materials differ in step edge coverage, as thoroughly characterised elsewhere.[13,15,49]

Electrochemistry

CV was carried out using a standard three-electrode configuration with a 760C potentiostat (CH Instruments, Inc.) essentially as described in our recent study.[14] Briefly, the HOPG sample was connected as the working electrode, a Pt wire served as the counter electrode and an insulated Ag wire (0.25 mm diameter), with AgCl deposited at the exposed disc-shaped end, acted as the reference electrode. In each experiment, a 20 µL droplet of solution containing the redox mediator of interest in 1 M KCl was placed on the HOPG surface (either *within seconds* of being freshly cleaved or after exposure to air for 1 or 12 h) with the other electrodes carefully immersed in the droplet. The droplet area was typically 0.18 – 0.21 cm^2, but precisely determined in each experiment as described in the SI, Section S1. Voltammetric scan rates spanned from 0.1 to 10 V s^{-1}. For the potential range used, electrowetting was not detected, but electrowetting can be seen at more positive potentials, which we shall report on later.

The diffusion coefficients of $FcTMA^+$ (1.5 mM in 1 M KCl) and $FcTMA^{2+}$ were determined from double potential step chronoamperometry at a Pt disc UME that served as the working electrode and a chloridized Ag wire as the quasi-reference counter electrode. More details are given in the Supporting Information (SI, Section S2).

Theory: model and analysis

The initial part of the model for this study was adapted and developed from that formulated by Wopschall and Shain.[50] For simplicity, it is assumed that only solution redox molecules undergo ET. This simplification was introduced to limit the number of adjustable parameters in the simulation, *i.e.* we did not wish to introduce a parallel set of kinetics for surface bound species. It does not affect the broad conclusions of the simulation results for a redox couple characterized by fast kinetics (*vide infra*). Furthermore, only the reduced form, Red, present in bulk solution adsorbs at the electrode surface, which is relevant to our study, which is in equilibrium with its solution counterpart in the near-electrode layer at any instant (rapid adsorption/desorption). The surface processes are:

$$Ox + e \rightleftharpoons Red$$
$$Red_{sol} \rightleftharpoons Red_{ads}$$

We employed a Butler-Volmer formulation for the electrode kinetics with a high ET rate constant so that the ET kinetics was essentially reversible, which is reasonable for the fast $FcTMA^{2+/+}$ system (*vide infra*). A Langmuirian adsorption isotherm was assumed, however, in some cases we also considered allowing the equilibrium adsorption constant to vary with the electrode potential to cover more complex adsorption cases. With this, the boundary value problem can be formulated as follows.

The diffusion equation (eq 1) to be solved for Red and Ox is of the form

View Article Online
DOI: 10.1039/C5CP06325F

$$\frac{\partial c_i}{\partial t} = D_i \frac{\partial^2 c_i}{\partial x^2} \quad (1)$$

where i = Red or Ox. Boundary conditions at the electrode surface (x = 0) are formulated in eq 2 - 4:

$$\mathbf{n.N}_{\text{Red}} = k_0\left(c_{\text{Red}} \exp[\frac{(1-\alpha)F}{RT}(E-E^{0\prime})]\sqrt{b^2-4ac} - c_{\text{Ox}} \exp[-\frac{\alpha F}{RT}(E-E^{0\prime})]\right) + \frac{d\Gamma}{dt} \quad (2)$$

$$\mathbf{n.N}_{\text{Ox}} = -k_0\left(c_{\text{Red}} \exp[\frac{(1-\alpha)F}{RT}(E-E^{0\prime})] - c_{\text{Ox}} \exp[-\frac{\alpha F}{RT}(E-E^{0\prime})]\right) \quad (3)$$

$$\Gamma = \Gamma_{\max} K(E) c_{\text{Red}} / (1 + K(E) c_{\text{Red}}) \quad (4)$$

Boundary conditions in the bulk of solution ($x \rightarrow \infty$) are formally the same as the initial conditions and are given in eq 5 and 6.

$$c_{\text{Red}} = c_0 \quad (5)$$

$$c_{\text{Ox}} = c_{\text{Red}} \exp[\frac{F}{RT}(E_{\text{in}} - E^{0\prime})] \approx 0 \quad (6)$$

Here, k_0 is the standard heterogeneous rate constant (set to be high; see below), α = 0.5 is a reasonable transfer coefficient for a fast outersphere redox couple, Γ is the surface concentration of adsorbed species at a given time (potential), $\Gamma_{\max}$ is the (maximum) surface concentration corresponding to a monolayer, c_0 is the initial/bulk concentration of the reduced form, $E^{0\prime}$ is the formal potential, E_{in} is the initial potential, and **n.N** is the diffusional flux, with F, R and T being the Faraday constant, the universal gas constant, and absolute temperature.

The potential-dependent equilibrium adsorption constant is defined by eq 7-9:[50]

$$K(E) = K_1 \exp[-\sigma n F (E - E^{0\prime}) / RT] \quad (7)$$

$$K_1 = K_0 \exp[0.4 \sigma n F / RT] \quad (8)$$

where K_0 is a potential-independent equilibrium constant which is related to the intrinsic adsorption constant, written in terms of activity:

$$K_i = \exp[-\Delta G^{\circ}_{\text{ads}} / RT] \quad (9)$$

The parameter σ sets the potential dependency of K; when σ = 0, K simply becomes K_0. Potential dependency of K was introduced for two reasons: i) it is plausible that the potential may influence the adsorption constant. For example, during the forward potential sweep (oxidation of $FcTMA^+$), the electrode acquires more positive charge, and that could cause the equilibrium constant to decrease due to electrostatic repulsion of adsorbed $FcTMA^+$; ii) it helped to demonstrate the applicability and the limits of the analytical approach presented herein for more complex adsorption scenarios. The factor 0.4 from the choice of a standard state where ΔG_{ads} does not depend on potential.[50]

We retained the differential formulation and solved the boundary value problem numerically using Comsol Multiphysics 4.4 (Comsol AB, Sweden). The analysis of the voltammetric results focused on a parameter that could easily be extracted from the experiment: the difference between the peak current $i_{\text{p,tot}}$ of the forward wave with adsorption (in the theory or in experimental data) and the theoretical one due to diffusion only, $i_{\text{p,diff}}$. We denote this difference as Δi_{p}. Of course, one has to know the diffusion coefficient of the Red species to calculate $i_{\text{p,diff}}$ accurately, which we discuss below. The approach is reasonable for the redox couples of interest because the electrode kinetics is fast and the peaks well-defined.

It turned out (see below) that Δi_{p} scales linearly with the scan rate v. This is expected for the peak current for a system comprising *only* a reversible surface-confined redox species, with the slope of i_{p} *vs* v being $n^2F^2\Gamma_0/4RT$.[51] Within good practical precision (its limits are discussed below) the plot of Δi_{p} *vs* v proved to have the same slope, so we can write

$$\Delta i_p = \frac{n^2 F^2 \Gamma_{\text{recov}}}{4RT} v \quad (10a)$$

$$\Gamma_{\text{recov}} \approx \Gamma_{\text{in}} \quad (10b)$$

We use the subscript "in" to denote the initial surface concentration or initial fractional coverage ($E = E_{\text{in}}$) and it is the input/known value used in the modelling. The subscript "recov" refers to the value of the initial surface concentration (or initial fractional coverage) that is recovered (or obtained) from the analysis of the modelling or experimental data.

The simple functional relation conveyed in eq 10 does not seem necessarily obvious when one considers the redox reaction of adsorbed species that are in equilibrium with their solution counterparts at any instant and thus the amount of adsorbed molecules changes as the potential sweep proceeds, in contrast to the case were the redox system (Red/Ox) are totally surface-confined. In the following, we present a simple formalism explaining this coincidence for the case of potential-independent K.

To simplify the analysis herein, we assume that the overall process is simply the sum of the two discrete components: adsorption and diffusion. Clearly, this assumption holds under conditions that favours low coverage like low bulk concentration and/or low equilibrium constant (weak adsorption). For this aspect of the analysis, we consider that a Langmuirian equilibrium holds at any moment of time between adsorbed Red and Red in the immediate vicinity of the electrode. To underline that the equilibrium constant does

View Article Online
DOI: 10.1039/C5CP06325F

not depend on potential in this part of the treatment we re-write eq 4 as follows:

$$\Gamma_{\text{Red}} = \Gamma_{\text{Red,max}} \frac{K_0 c_{\text{Red}}}{1 + K_0 c_{\text{Red}}} \quad (11)$$

A Nernstian relation also holds at any time for the concentrations of Ox and Red at, and just near, the electrode surface (eq 12):

$$\frac{c_{\text{Red}}}{c_{\text{Ox}}} = e^{-f\eta} \quad (12)$$

where $f = nF/RT$ and $\eta = E - E^{0\prime}$.

With the assumption above applicable at, and immediately close to, the electrode surface (by electrode surface we imply the plane where the concentration gradients, owing to diffusion, originate) the sum of concentrations of redox molecules is equal to the total concentration c_0 that in our case is the bulk concentration of Red (eq 13).

$$c_{\text{Red}} + c_{\text{Ox}} = c_0 \quad (13)$$

Therefore eq 12 can be expressed as

$$c_{\text{Red}} = \frac{c_0 e^{-f\eta}}{1 + e^{-f\eta}} \quad (14)$$

During the potential sweep, c_{Red} obviously changes according to the electrode potential, however, the effect of the assumption we make is that there is no "stripping" of Red_{ads} from the electrode surface, rather it is converted to Ox. The goodness of this assumption is tested and shown to be reasonable in the SI (Section S3). With this in mind, c_{Red} from eq 14 can be substituted into eq 11 to get

$$\Gamma_{\text{Red}} = \Gamma_{\text{Red, max}} \frac{K_0 c_0 e^{-f\eta}}{1 + (1 + K_0 c_0) e^{-f\eta}} \quad (15)$$

To obtain the expression for current due to adsorbed species, one takes the time derivative of eq 15:

$$\frac{i_{\text{ads}}}{nF} = -\frac{d\Gamma_{\text{Red}}}{dt} = \Gamma_{\text{Red, max}} \frac{K_0 c_0}{(1 + K_0 c_0)^2} \frac{-fve^{-f\eta}}{((1 + K_0 c_0)^{-1} + e^{-f\eta})^2} \quad (16)$$

where v, the scan rate, appears outside the exponent as a result of differentiating η with respect to time. By noting that $\Gamma_{\text{Red, in}} = \Gamma_{\text{Red, max}} K_0 c_0 / (1 + K_0 c_0)$, where $\Gamma_{\text{Red, in}}$ is the surface concentration prior to the potential sweep, eq 16 can be re-written as

$$\frac{i_{\text{ads}}}{nF} = -\frac{d\Gamma_{\text{Red}}}{dt} = \Gamma_{\text{Red, in}} (1 + K_0 c_0)^{-1} \frac{-fve^{-f\eta}}{((1 + K_0 c_0)^{-1} + e^{-f\eta})^2} \quad (17)$$

However, we are not interested directly in the expression for current, rather we want to obtain the formula for the peak current. Differentiating eq 17, setting it to zero and solving the resulting algebraic equation, one finds:

$$e^{-f\eta_p} = (1 + K_0 c_0)^{-1} \quad (18)$$

where η_p is the peak overpotential. Substituting this in the equation for the current (eq 17) one finally obtains the formula for the peak current (eq 19), which is identical to that of surface-bound reversibly reacting redox molecules as mentioned in the text above:

$$i_{\text{ads,p}} = \frac{n^2 F^2 \Gamma_{\text{Red,in}} v}{4RT} \quad (19)$$

This derivation serves as a proof that the initial coverage can be found by the method proposed in this paper under the conditions when the approximations made hold. Attempting to apply a similar strategy to the case of potential-dependent K is more complicated (and is not considered) because one has to account for "stripping" of Red_{ads} during the potential sweep and its accumulation in the pre-electrode layer, but "the stripping" of Red_{ads} follows not only the change in c_{Red} near the electrode but also the change in K with applied E. In the following, we present the results of numerical modelling first for the case of potential-independent K to corroborate the simple theory described above, and then the case of potential dependent K will be considered.

CVs both with the adsorption of Red and without (pure diffusional process) were computed at different scan rates by solving eq 1 – 6 (obviously Γ was set to zero for the diffusion-controlled case). The CVs with adsorption are shown in Figure 1a (diffusional CVs, which are well-known, are not shown for clarity). The difference plot for the forward waves obtained by subtraction of CVs without adsorption from those with adsorption (i_{tot} - i_{diff}) is given in Figure 1b. The charge Q under each difference curve and Δi_p are plotted in Figure 1c and d, respectively. The model parameters were assigned the following numerical values: $D_{\text{Red}} = 6.7 \times 10^{-6}$ cm^2 s^{-1}, $D_{\text{Ox}} = 6.2 \times 10^{-6}$ cm^2 s^{-1}, $c_0 = 0.25$ mM, $k_0 = 5$ cm s^{-1}, $\alpha = 0.5$, $E^{0\prime} = 0.38$ V, $E_{\text{in}} = 0$ V, $n = 1$, $\Gamma_{\text{max}} = 5 \times 10^{-10}$ mol cm^{-2} (close to an earlier estimate[38]), and $\Delta G°_{\text{ads}} = -14.2$ kJ mol^{-1} (a reasonable value for physisorption[52]). This corresponds to an initial surface concentration $\Gamma_{\text{in}} = 2.2 \times 10^{-11}$ mol cm^{-2} (4.4% of a monolayer) and $K_i = 305$ ($K_0 = 183$ cm^3 mol^{-1}, given that 0.604 is the mean molar activity coefficient of 1 M KCl).[53]

In order to recover Γ_{in}, one can, in principle, use either the charge under the (voltammetric) difference curve or Δi_p. At first glance, the former might appear a more attractive quantity for analysis as it "accounts" for the whole difference between the two waves (with and without adsorption) and does not necessitate making model assumptions about adsorption (like the isotherm type), as long as the intrinsic assumption about decoupled diffusion and adsorption holds. However, the coverage recovered from the charge data resulted in an underestimate of the actual amount by about 11% ($\Gamma_{\text{recov}} = 1.96 \times 10^{-11}$ mol cm^{-2}). Moreover, given that the difference curves obtained from the experimental data would be less ideal in shape than depicted in Figure 1b, an analysis based on charge would very likely increase the error.

View Article Online
DOI: 10.1039/C5CP06325F

Journal Name

ARTICLE

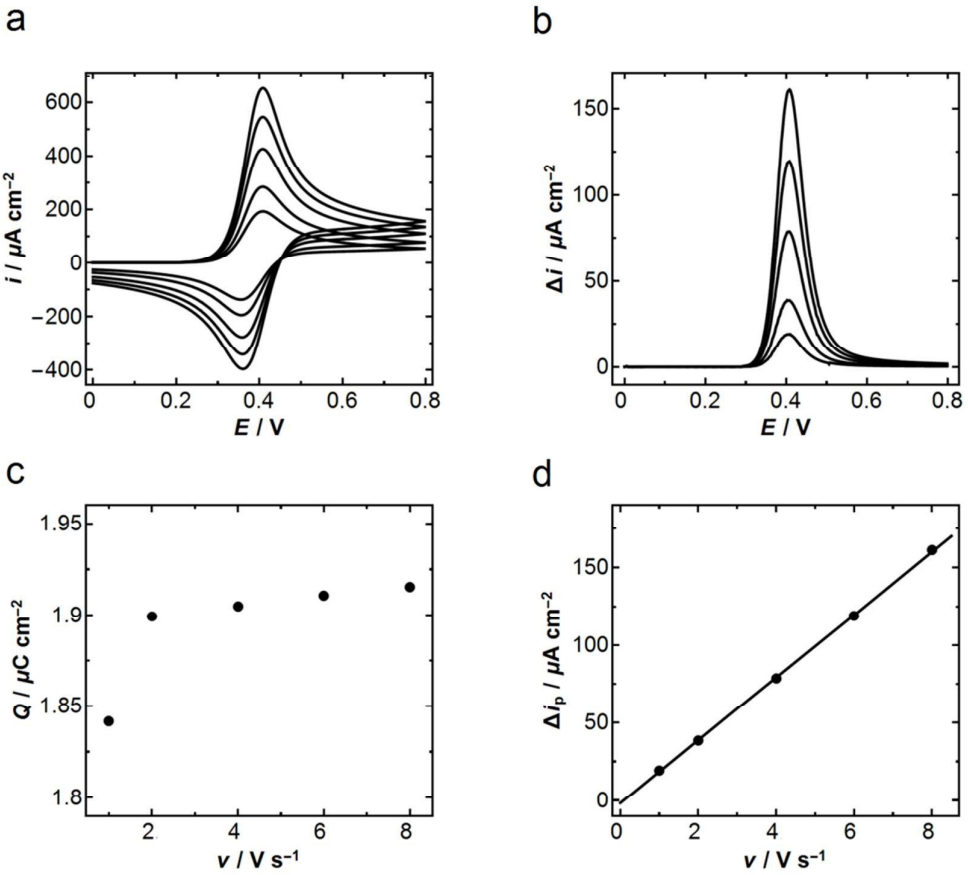

Figure 1. *a*) A series of computed diffusional CVs complicated by adsorption of Red at scan rates of 1, 2, 4, 6 and 8 V s^{-1} (values of all parameters in the simulation are listed in the text). *b*) Difference plot for the forward waves (smaller currents) of CVs shown in *a* ($\Delta i = i_{tot} - i_{diff}$); *c*) Charge under each difference curve shown in *b* plotted *vs* scan rate. *d*) Peak current difference (as defined in the text) for the forward wave plotted *vs* scan rate for each CV shown in *a*.

For the case presented in Figure 1, eq 10 was used to determine the coverage (in particular the data from Figure 1d), resulting in Γ_{recov} = 2.15 × 10^{-11} mol cm^{-2}, which is only slightly different from Γ_{in} (2.2% less). Both methods underestimate the actual surface coverage, but evidently, charge is worse for the analysis of the full voltammetric wave. It is impressive that the peak current is so accurate but, of course, under different conditions the error might become higher and so we further explored the capability of the model to recover Γ_{in} for a broad range of fractional coverages ($\theta_{in} = \Gamma_{in}/\Gamma_{max}$).

The analysis just-described was extended to bulk concentrations of Red varying from 0.25 mM to 55 mM, which covered the range of θ_{in} from 0.04 to 0.91, with the values of other model parameters given above remaining unchanged. The deviation of Γ_{recov}, or equivalently θ_{recov}, from its set value was measured with the quantity $\log_2 \theta_{recov}/\theta_{in}$. A unit of this quantity corresponds to a two-fold deviation of θ_{recov} from θ_{in} and it is convenient to compare errors that go on both sides of a reference quantity (as will become clear below). As can be appreciated from Figure 2, curve *1*, the error remains rather small up to θ_{in} ~ 0.7 but rapidly increases beyond this point, indicating an approximately two-fold underestimate of θ_{in} when θ_{in} ~ 0.9. Evidently, at higher coverages, diffusion is more significantly affected by the adsorption/desorption process occurring at the electrode surface and the overall process can no longer be represented as the mere sum of the two.

We further tested the applicability of eq 10 for the case of potential-dependent *K*, relying on the results of the numerical calculations. As mentioned above, the parameter σ determines the sensitivity of *K* towards the change in potential but it also affects the magnitude of *K* (eq 8) so Γ_{in} changes with σ even for

View Article Online
DOI: 10.1039/C5CP06325F

the same E_{in}. For σ in the range of 0 – 0.5, θ_{in} covered a similar range of values as in the previously treated potential-independent K case (with c_0 = 0.25 mM). CVs were computed for each value of σ by solving eq 1 – 9 at different scan rates and Γ_{recov} was determined from Δi_p. As in the case of potential independent K, Δi_p proved to scale linearly with v, however, in this case Γ_{recov} obtained from eq 10 deviated more strongly from Γ_{in}. The error in terms of recovered θ_{in} is presented in Figure 2, curve *2*. Unlike the previous case, the error increases significantly with σ, even for small σ, and reaches a maximum at intermediate values of σ. At the maximum, θ_{recov} overestimates θ_{in} by more than three times. The fact that the error diminishes at higher σ is probably due to that θ_{in} approaches a limit of unity with increasing σ, whereas θ_{recov} scales at a slower pace with σ. It should be emphasized that Δi_p followed the linear relation with v for *all* the conditions tested (with K being or not being a function of potential), regardless of the error in the estimation of Γ_{in}.

We imitated, by simulation, an experiment aimed at generating an adsorption isotherm for σ = 0.13 (close to the maximal error in Γ_{in}) by plotting Γ_{recov} *vs* c_0. The results followed the Langmuir equation (perfect straight line of $1/\Gamma_{recov}$ *vs* $1/c_0$ coordinates) but, of course, the slope and the intercept were different from the respective input values. Thus, it is not possible to distinguish when K is and when it is not a function of potential based on the proposed methodology. However, to reiterate the proposed analysis works well for lower to moderate surface concentrations (up to θ_{in} ~ 0.5), for potential independent K which applies to a wide range of systems).

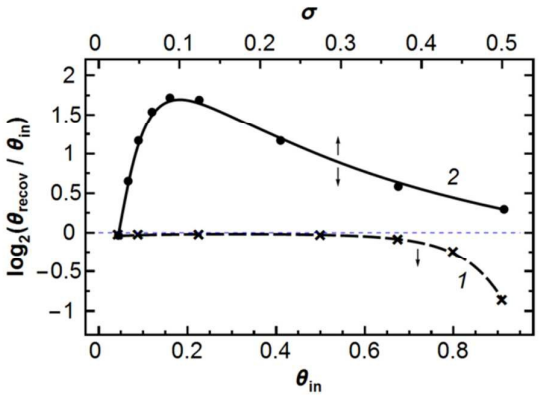

Figure 2. Error in ϑ_{in}, as defined in the text, recovered by the model for the case of potential-independent K (curve *1*) and potential-dependent K (curve *2*). The arrows indicate that curve *2* is plotted *vs* σ and ϑ_{in} but curve *1* only *vs* ϑ_{in}. The lines serve only for eye-guidance.

In the course of our experimental work, it turned out that the adsorption isotherm of $FcTMA^+$ on HOPG is not strictly Langmuirian, but is more reminiscent of the Frumkin isotherm with attractive lateral interaction, especially noticeable at higher bulk concentrations (higher surface concentratons). Naturally, a question was whether it is possible to obtain reasonable initial coverages if the system follows a different, not Langmuir, isotherm. The detailed discussion of the experimental results will follow in the next section and here, in the last part of the theoretical section, we treat the case where the system follows the Frumkin isotherm with potential-independent K.

The treatment is similar in principle to the one for the case of the Langmuir isotherm. The equation for the adsorption of the Red species now reads:[54]

$$\theta_{Red} = \frac{K_0 c_{Red} e^{-g\theta_{Red}}}{1 + K_0 c_{Red} e^{-g\theta_{Red}}} \quad (20)$$

where g is a parameter characterizing the lateral interaction of the adsorbate molecules. It is attractive when g < 0 and repulsive when g > 0. Assuming fast electron transfer kinetics and combining eq 14 and eq 20, we have:

$$\theta_{Red} = \frac{K_0 c_0 e^{-f\eta - g\theta_{Red}}}{1 + e^{-f\eta} + K_0 c_0 e^{-f\eta - g\theta_{Red}}} \quad (21)$$

The expression for the current for the adsorbed Red is obtained by differentiating eq 21

$$\frac{d\theta_{Red}}{dt} = -\frac{K_0 c_0 e^{-f\eta + g\theta_{Red}} (g(1 + e^{-f\eta})(d\theta_{Red}/dt) + fv)}{(1 + e^{-f\eta + g\theta_{Red}} + K_0 c_0 e^{-f\eta})^2} \quad (22)$$

and solving the resulting eq 22 for $d\theta_{Red}/dt$. For clarity, the notation can be simplified by putting $q = e^{-f\eta}$, $r = e^{g\theta}$, $K_0 c_0 = C$ and removing the subscript "Red". Thus, the equation for the current reads:

$$\frac{i_{ads}}{nF\Gamma_{max}} = -\frac{d\theta}{dt} = Cfvrq / (r^2(1+q)^2 + C(2+g)rq(1+q) + C^2q^2) \quad (23)$$

Next, eq 23 needs to be differentiated and set to zero (in fact, only the numerator). It contains $d\theta/dt$ that can be excluded by invoking eq 22. The result is eq 24 that includes not only η but also θ, both are in the exponent. To ease handling, we employed Mathematica 10.[55]

$$r^4 + 2Cq^2gr^3 - 2qr^3(p+C) + q^4\left(r^2 + C(2+g)r + C^2\right)^2 + q^3r\left(2r^3 + 2C(3+2g)r^2 + C^2r(6+g(4+g)) + 2C^3\right) = 0 \quad (24$$

Thus, one has to solve simultaneously eq 24 and 21 to obtain η and θ for the peak current. This system can only be solved numerically due to the complicated and transcendental form of these equations. Before we proceed with the numerical solution and analysis, it is worthwhile to show that the peak current is always proportional to the scan rate (as in the case of the simple Langmuir isotherm). The current, as defined by eq 23, can be presented as a product of v and some function of $r = r(\theta)$, q, C, and g:

$$\frac{i_{ads}}{nF\Gamma_{max}} = fvF_1(r(\theta), q, C, g) \quad (25)$$

It is worthwhile re-writing eq 21 with newly introduced symbols:

View Article Online
DOI: 10.1039/C5CP06325F

$$\theta = \frac{Cqr(\theta)^{-1}}{1+q+Cqr(\theta)^{-1}} \quad (26)$$

The system of simultaneous equations 24 and 26 can be solved, in principle, for q and θ, with the solution being dependent only on C and g, as the equations in question contain only these two parameters and integers. This fact can be written in a general form:

$$\begin{aligned} q_p &= F_2(C,g) \\ \theta_p &= F_3(C,g) \end{aligned} \quad (27)$$

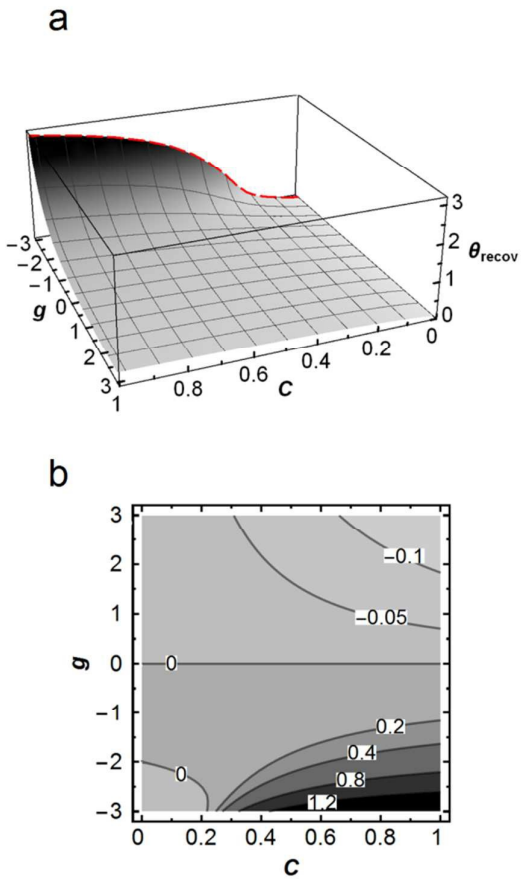

Figure 3. *a*) Recovered Frumkin isotherms for a range of g values. Red dashed border delineates the shape of the isotherm for g = -3. *b*) Error in recovery ϑ_{in} for Frumkin isotherms, as defined in the text.

where the subscript "p" refers to the peak values of the quantities. When these are substituted in eq 25, it can be seen that F_1 will only contain C and g (eq 28) and not v or any parameters depending on it. Therefore, the peak current is always proportional to v as we pointed above.

$$\begin{aligned} \frac{i_{ads,p}}{nF\Gamma_{max}} &= fvF_1(r(\theta_p), q_p, C, g) \\ &= fvF_1(r(F_3(C,g)), F_2(C,g), C, g) \\ &= fvF_4(C,g) \end{aligned} \quad (28)$$

When examining eq 23, this result is not obvious, as each differentiation of q "releases" v as a factor only for the terms containing q. v becomes a common factor in the resulting expression when $d\theta/dt$ is substituted into it (as was already mentioned above) and in this way v plays no role when this expression is set to zero.

The expression for peak current is, in general form, given by eq 28, which can be written in slightly different form:

$$\frac{4i_{ads,p}}{fnF\Gamma_{max}} = 4vF_4(C,g) \quad (29)$$

It follows from eq 29 that $4F_4$ is a slope of the adsorption current (as normalized) when plotted *vs* v. By comparing eq 29 with eq 10, we can identify $4F_4$ with θ_{recov}. Thus θ_{recov} can be found for every pair, C and g.

It is convenient, as in the case with the Langmuir isotherm, to explore how the recovered initial coverage deviates from the set initial coverage by plotting the error as $\log_2(\theta_{recov}/\theta_{in})$ with θ_{in} determined by solving eq 20 numerically and bearing in mind that, in this case, $K_0c_{Red} = K_0c_0 = C$. The error plot for a range of C and g, along with recovered isotherms are given in Figure 3. Frumkin isotherms have an inflexion point for $g < 0$ and this appears on the slices of the surface plotted in Figure 3. Therefore, the methodology and analysis suggested in this paper (essentially based on eq 10 and its elaboration) allows one to restore the Frumkin isotherm to some degree. The precision with which this restoration can be achieved depends on particular values of C and g. By examining the plot in Figure 3b, one can notice that the error becomes significant on the negative side of g and generally at higher C, resulting in unrealistic θ_{recov} values. At the extreme of low C (< ~ 0.25) the isotherm can be recovered with great precision. This region lies approximately before the inflexion point on the recovered isotherm. Therefore, one generally expects much better recovery of the initial coverage (and the isotherm) before the inflexion point of the recovered isotherm. Note that there is little error in recovery θ_{in} when g = 0, which confirms the previously treated case for the Langmuirian isotherm, with potential-independent K.

Experimental Results and Discussion

It was not the purpose of this study to perform detailed mechanistic research of the adsorption of ferrocene derivatives on HOPG. Rather, we intend to present an account of the *relative* extent of adsorption of various ferrocence derivatives on HOPG under several experimental conditions so as to draw general conclusions as to such effects in contemporary studies of carbon electrodes. Based on the

View Article Online
DOI: 10.1039/C5CP06325F

analysis above, voltammetric measurements suffice for this purpose and provide robust values for surface coverages.

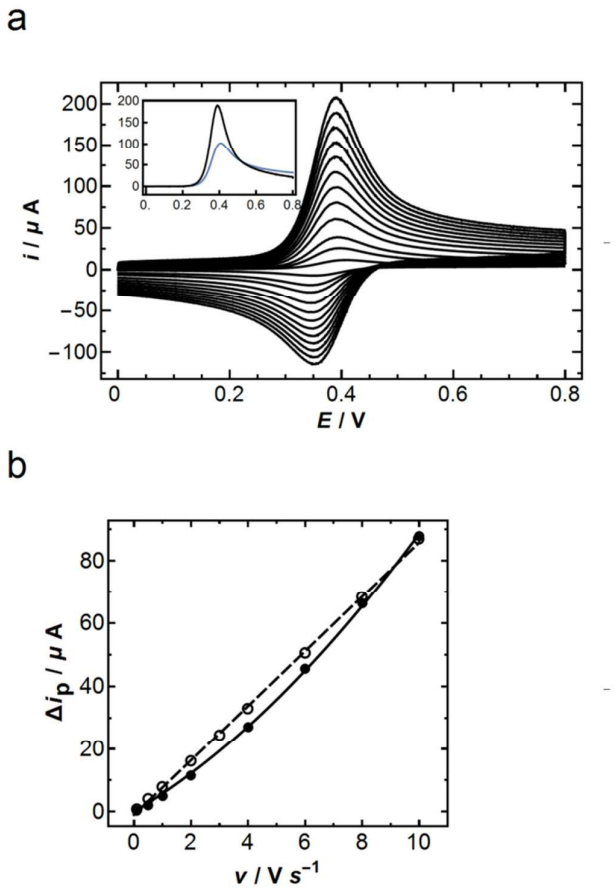

Figure 4. *a*) CVs for the oxidation of 0.25 mM $FcTMA^+$ in 1 M KCl at freshly cleaved AM grade HOPG with scan rates of 0.1, 0.5 and 1 – 10 V s^{-1} (with an increment of 1 V s^{-1}). The inset shows the experimental forward wave at 10 V s^{-1} (black) compared with the corresponding computed diffusional wave (blue), crossing at *ca*. 0.55 V *b*) Peak current difference Δi_p plotted *vs* scan rate. Filled circles are for $FcTMA^+$ data from the CVs presented in *a* with the fit to a second-order polynomial $y(x) = C_1x + C_2x^2$. Open circles are for FcCOOH (0.25 mM in 1 M KCl) with the fit to a straight line. Electrode areas were *ca*. 0.2 cm^2.

The model presented in this article is based on the relation of the difference between the experimental and theoretical peak currents as the function of scan rate and, to the best of our knowledge, there has not been a similar simple and straightforward method of quantitative processing of CVs complicated by weak adsorption. An approach for extracting surface coverage from a single CV measurement, based on semi-integration, has been suggested,[56] however, a fundamental premise of this method was a concomitant presence of both the reduced and oxidized forms in the adsorbed state in equilibrium. Apparently the formalism developed for this approach is applicable only when this assumption holds. We tested this method for the conditions relevant to our case and found that the initial concentration of Red_{ads} returned by this model was almost five times higher than the input/expected value (see SI, Section S4 for details).

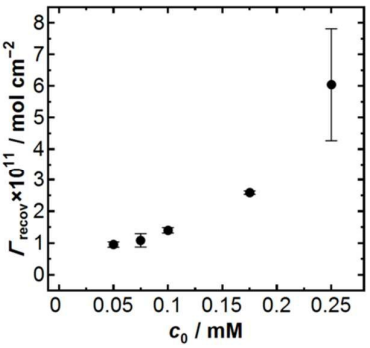

Figure 5. Empirical adsorption isotherm of $FcTMA^+$ at freshly cleaved AM HOPG surfaces.

Typical voltammetry of $FcTMA^{+2/+}$ at HOPG at a bulk concentration of 0.25 mM, for a range of scan rates, from 0.1 V s^{-1} to 10 V s^{-1}, is presented in Figure 4a. It is noticeable that the peak currents of the forward waves are higher than those of the reverse waves and far exceed the values expected for pure diffusional waves. The inset in Figure 4a contrasts the experimental forward wave with the computed one for a pure diffusional response at 10 V s^{-1}. This voltammetric behaviour, where the experimental peak current is more than twice that predicted for a simple diffusion-limited process (no adsorption), is a clear signature of some adsorption of the reactant,[50] with the product diffusing into solution (as evidenced by the much smaller return peak). Furthermore, the crossing of the experimental curve and simulated diffusion-limited response illustrates the problem of taking the difference in the charge between experiment and simulation, for the particular case of weak adsorption, which applies here.

The peak current difference plotted vs scan rate for the voltammetric data shown in Figure 4a is given in Figure 4b. The diffusion coefficients used to calculate i_p were either determined experimentally or adopted from the literature (see SI, Section S2, for details). The obtained dependency between Δi_p and v was not quite linear for $FcTMA^+$, but all FcCOOH experiments yielded the expected straight lines (the same figure). Strictly, we cannot extract surface concentrations from non-linear plots. However, the behaviour at higher scan rates may be more complicated by background/capacitative charging (see SI, Section S5), which may have a coverage-dependent character and therefore not manifested as a standard background/blank voltammogram (for pure electrolyte solution). Because the Δi_p vs v plot for $FcTMA^{2+/+}$ was not quite linear, it was fitted to a second-order polynomial of the type $y(x) = C_1x + C_2x^2$ and the coefficient C_1 was identified with the slope as defined by eq 10. In other words, only slow scan rates were employed to extract surface concentrations.

The surface concentration of $FcTMA^+$ determined for bulk concentrations in the range 0.05 – 0.25 mM is summarized in Figure 5, which represents an empirical isotherm of adsorption of $FcTMA^+$ at the fresh surface of HOPG. As expected, Γ_{recov}

View Article Online
DOI: 10.1039/C5CP06325F

increases with c_0 but it seems to have a convex shape instead of a concave one – typical for Langmuir or Temkin isotherms. This is suggestive of a Frumkin type isotherm with attractive interaction between adsorbate molecules. Although, at first glance, this might appear unusual for positively charged $FcTMA^+$ that should experience repulsive coulombic interaction, counteranions could promote such an interaction. For example, attractive lateral interaction between neutral ferrocene molecules adsorbed on Ag(100) surface has been reported.[57] Also, co-adsorption of counterions or anions of an indifferent electrolyte are known to take place in some electrochemical systems[54,58,59] It is also worth pointing out that adsorbent-adsorbate interactions, and consequently isotherms, relevant to electrochemical studies are difficult to describe and compute on electrode surfaces.[54]

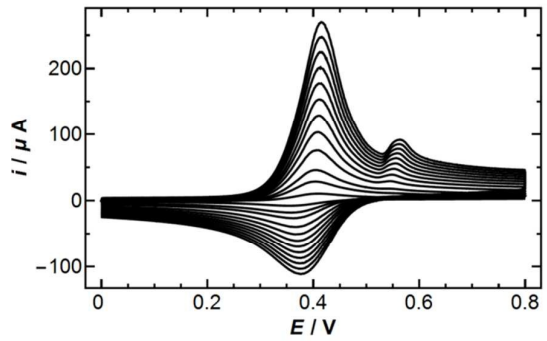

Figure 6. CVs for the oxidation of 0.25 mM $FcTMA^+$ in 1 M KCl at a sample of AM HOPG "aged" in air for 1 h. The scan rates were 0.1, 0.5 and 1 – 10 V s^{-1} (with increment of 1 V s^{-1}).

We have shown previously that exposure of cleaved HOPG to the atmosphere can have a significant impact on the voltammetry of several redox processes,[15,16,23,60] which we attributed to surface contamination, delamination, oxidation and other factors[15,16,23] We were interested in elucidating whether such effects were manifest in $FcTMA^+$ adsorption. Exposure of AM HOPG to air for 1 h prior to electrochemical measurements produced a notable effect on the degree of adsorption. Representative voltammetry of such samples is shown in Figure 6. Thus for c_0 = 0.25 mM, the amount of weakly adsorbed $FcTMA^+$ constituted $\Gamma_{recov} = 1.1 \times 10^{-10}$ mol cm^{-2}, which is almost twice the amount adsorbed on freshly cleaved AM HOPG. This could be attributed to the accumulation of $FcTMA^+$ in an airborne contaminating film at HOPG.[15,16,61,62] Also, a small "hump" appeared at more driving potentials, suggesting the oxidative stripping (to $FcTMA^{2+}$) of strongly adsorbed $FcTMA^+$, the amount of which was estimated to be 1×10^{-11} mol cm^{-2}. It appears that, under these conditions, the HOPG surface is heterogeneous, comprising sites with different $FCTMA^+$ adsorption energies. This could be due to some non-uniformity of the contaminating film and/or delamination of the topmost layers, the significance of which for electrochemistry was established in our previous work.[15,23]

Although a range of techniques are routinely applied to understand the quality of HOPG surfaces,[15,16,23,61,62] it follows that the adsorption of ferrocene derivatives could provide a simple probe of surface contamination, although extensive experiments would be needed to conclusively prove the link between surface contamination and ferrocene adsorption, beyond that for a pristine surface that we have mainly focused on for this paper (see also below).

Although SPI-3 HOPG has much higher density of step edges than AM grade (by at least two orders of magnitude[15,42,49]), this had no effect on the degree of adsorption of $FcTMA^+$ on a freshly cleaved surface. Thus, for 0.25 mM $FcTMA^+$, the measured adsorbed coverage was Γ_{recov} = (5.5 ± 0.9) × 10^{-11} mol cm^{-2} at a freshly cleaved SPI-3 surface, and this value was practically unchanged at a sample exposed to air for 12 h (Γ_{recov} = 5.6 ± 0.6) × 10^{-11} mol cm^{-2}).

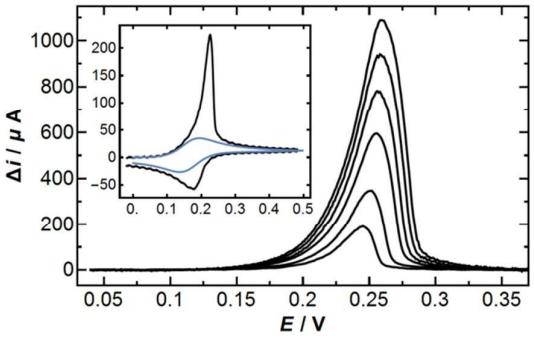

Figure 7. a) Difference plot ($\Delta i = i_{tot} - i_{diff}$): forward waves for 0.25 mM $FcCH_2OH$ at a freshly cleaved AM HOPG with a scan rate of 0.1, 0.5 and 1 – 10 V s^{-1} (with increment of 1 V s^{-1}). The inset shows a full experimental CV (black) and a computed diffusional one (blue) for v = 1 V s^{-1}.

Two highly significant points can be made from these results. First, the adsorption of $FcTMA^+$ on freshly cleaved (pristine) HOPG surface does not depend on the amount of step edges present. Indeed, the coverages on both AM and SPI-3 grades are the same within experimental error. This is in line with our previous work on the adsorption of anthraquinone-2,6-disulfonate.[42] Second, the fresh and "aged" surfaces of SPI-3 grade HOPG exhibited the same degree of $FcTMA^+$ adsorption. This could suggest that SPI-3 grade HOPG is less prone to the formation of airborne contaminating films, which is reasonable because SPI-3 grade HOPG is characterized by extremely short terrace widths (31% of surface being step edges[42]), which would impedes the formation of continuous contaminant films across the basal surface.

Voltammetry of the other two ferrocene derivatives on freshly cleaved HOPG also indicated adsorption that is summarised in Table 1 along with $FcTMA^+$ data. The data for $FcCH_2OH$ at the freshly cleaved AM HOPG suggest strong adsorption of the reduced molecular form, which is indicated by a high current of the forward wave in CV measurements. A few key features can be extracted from these data without over-analysis. The shape of the forward waves due to adsorption can be made clearer by subtracting the computed diffusion CVs from the experimental ones as is done in Figure 7. We are able to do this in this case, because adsorption is strong and the surface coverage of $FcCH_2OH$ on the HOPG

View Article Online
DOI: 10.1039/C5CP06325F

surface is high. The resulting current-potential difference plots have narrow peaks (the full width at half-maximum for 1 V s^{-1} wave is ~ 30 mV compared to 90.6 mV for non-interacting redox-active molecules in a monolayer, undergoing fast (reversible) electron transfer[63]). This indicates some potential-dependent character of adsorption and/or attractive lateral interaction between the adsorbate molecules.[63] The estimated charge under the forward profiles amounted to 5.5-7.0 μC cm^{-2}, depending on the scan rate, which gives a Γ_{recov} ~ 3.4 (± 0.5) × 10^{-10} mol cm^{-2}. With the value for a monolayer of ferrocene rings estimated[38] to be 4.6 × 10^{-10} mol cm^{-2}, and the very approximate character of our value, we can say that adsorbed $FcCH_2OH$ forms almost a complete monolayer at HOPG for a bulk concentration of 0.25 mM. This is reasonable, given the zero charge of this species, and one may well expect higher adsorption as compared to single-charged $FcTMA^+$ or $FcCOO^-$. FcCOOH existing in solution mostly in ionised form under the experimental conditions used herein (pK_a of the Red form[64] is 6.1) exhibited a voltammetric response typical for weakly adsorbed reactant. The value for surface concentration (Table 1) proved to be similar to $FcTMA^+$ for the same bulk concentration (0.25 mM). Given the negative charge on $FcCOO^-$ and that the potential of zero charge for graphite[65] is *ca.* -0.24 V vs Ag/AgCl, 1 M KCl, this suggests that coulombic effects between the electrode and ferrocene derivatives are not significant in determining the amount of adsorption of this species.

Table 1. Adsorption of ferrocene derivatives at HOPG, c_0 = 0.25 mM.

Sample	Mediator	Γ_{recov} / 10^{-11} mol cm^{-2}	Number of replicates
Fresh AM HOPG	$FcTMA^+$	6 ± 2	12
	$FcCOO^-$	6 ± 1.1	10
	$FcCH_2OH$	34	1
AM HOPG aged for 1 h	$FcTMA^+$	11.0 ± 0.2	3
Fresh SPI-3 HOPG	$FcTMA^+$	5.5 ± 0.9	3
SPI-3 HOPG aged for 12 h	$FcTMA^+$	5.6 ± 0.6	4

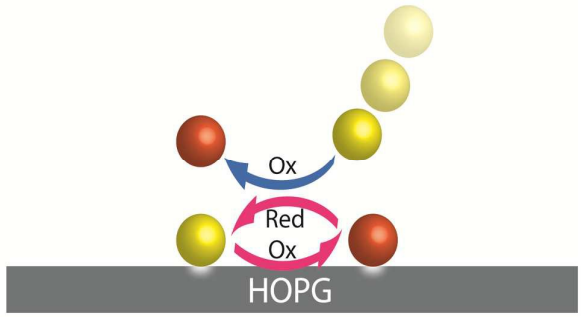

Figure 8. Schematic of mediated ET shows electron exchange between a molecule in the solution side and the one in adsorbed one. The latter undergoes ET with the electrode.

As mentioned in the introduction, adsorption phenomena can cause complications in the proper use of voltammetric standards and its consideration is essential in the interpretation of voltammetric data. Adsorption is not always obvious in macroscale CV measurements unless the scan rate is appropriately set, but may impact such voltammetric measurements in other situations. For example, a recent study[36] on ET kinetics and surface contamination effects, carried out with scanning electrochemical microscopy, did not consider the adsorption of $FcTMA^+$ on the HOPG used. Yet, its significance is clear and it could have an important impact on the correct analysis of such data.

Lastly, it is important to point out that recognition of the adsorption of ferrocene derivatives is important in the mechanistic interpretation of heterogeneous ET kinetics. Surface-confined ferrocenes are known to be able to exchange electrons with their solution counterparts:[66]

$$Ox^{z}_{ads} + e \rightleftharpoons Red^{z-1}_{sol}$$

Thus, if a ferrocene molecule M_{Ox} sits on the surface (in Ox state) it can exchange an electron with another ferrocene molecule M'_{Red} in the Red state from the solution and, thus, become M_{Red}, *i.e.* ET between the electrode and solution species is mediated by the adsorbed species (see schematic in Figure 8). With ferrocene derivatives evidently adsorbing on carbon (HOPG) electrode surfaces, one cannot easily separate mediated from direct ET using standard voltammetric measurements and one must recognize that such a mechanism may occur, may even dominate, and its extent will be potential-dependent and in competition with conventional heterogeneous outer sphere ET between the electrode and solution species. The competition between these different pathways will also change as the surface coverage changes with potential.

Conclusions

In this work, a simple methodology that allows the determination by cyclic voltammetry of the amount of weakly adsorbed redox species at an electrode has been developed and applied to the voltammetric study of adsorption of ferrocene derivatives on HOPG. Specifically, the difference in peak current of an experimental forward voltammetric wave and the peak current calculated based on diffusion-controlled redox reaction, serves as a measure of the amount of adsorbed reactant and is related to it through a well-known equation for surface-confined redox active species (eq 10 and 19). The applicability of this methodology was investigated for the case of Langmuirian and Frumkin adsorption isotherms. Low amount of adsorbed molecules, which can be achieved by keeping the bulk concentration of the adsorbate at a low level, was shown to impart the method with good practical precision for both types of the isotherms. However, if the system follows the Frumkin isotherm, the error tends to be larger. The case of a potential-dependent equilibrium constant was also investigated. In this case the error can be very large even at

View Article Online
DOI: 10.1039/C5CP06325F

low surface coverages and one cannot distinguish whether the system exhibits potential-dependency of the equilibrium constant, or not, within the proposed methodology.

The adsorption of three ferrocene derivatives has been studied on fresh and "air-aged" surfaces of two very different grades of HOPG. The freshly cleaved surface of the highest quality AM grade HOPG adsorbs the reduced forms of ferrocene derivatives in the following order: $FcTMA^+$ ~ $FcCOO^-$ < $FcCH_2OH$. The fact that both positively and negatively charged species adsorb to the same extent may suggest the co-adsorption of counteranions of the supporting electrolyte that somewhat screen the charge of the adsorbed species. An empirical adsorption isotherm of $FcTMA^+$ on fresh surfaces of AM grade HOPG was found to have convex shape, suggesting possible attractive lateral interaction of this reactant in the adsorbed state.

Adsorption of $FcTMA^+$ on fresh AM grade HOPG and SPI-3 grade HOPG was found to be the same within experimental error for the bulk value of $FcTMA^+$ c_0 = 0.25 mM. The "aged" surface of AM grade HOPG demonstrated notably higher capacity (by about a factor of two) to adsorb this redox molecule, along with a small fraction of strongly adsorbed $FcTMA^+$ - a feature absent on the fresh surface. This result may be understood in light of the formation of an air-borne contaminating film on the basal plane of AM grade HOPG that "traps" more of these redox molecules than the pristine surface, as well as other surface structure changes, such as oxidation. In contrast, "aged" SPI-3 grade HOPG did not manifest any increase in weakly adsorbed $FcTMA^+$ or any amount of strongly bound $FcTMA^+$, tentatively suggesting that the SPI-3 surface is much less prone to the formation of contaminating films, and surface modification, although further work is needed to prove this idea.

Lastly, we have outlined the importance and implications of considering the adsorption of ferrocene derivatives in studies of their ET kinetics at carbon electrodes. In one sense, the voltammetric response may well be influenced by the amount of adsorbed redox species, and if this is not recognized one may deduce incorrect physical parameters of the system. In another sense, adsorbed ferrocene derivatives can also mediate ET, which has to be recognized when analyzing data and deducing kinetic parameters.

List of symbols

C	dimensionless parameter K_0c_0
c_0	bulk concentration
$c_{Red/Ox}$	Space and time-dependent concentration of Red/Ox
$D_{Red/Ox}$	Diffusion coefficient of Red/Ox species
E	Electrode potential
$E^{0'}$	Formal electrode potential
E_{in}	Initial electrode potential
F	Faraday constant
f	nF/RT
F	a function defined by the context
g	parameter characterizing lateral interaction between adsorbate molecules
i_{ads}	Current due to reaction of adsorbed redox species
$i_{p,diff}$	Peak current in a purely diffusion-controlled CV
$i_{p,tot}$	Peak current on a diffusional CV complicated by adsorption of redox species
k_0	Standard heterogeneous rate constant of electron transfer
$K(E)$	Potential-dependent adsorption constant
K_0	Potential-independent adsorption constant under given conditions (cm^3 mol^{-1})
K_1	potential-independent part of $K(E)$
K_i	intrinsic potential-independent adsorption constant (dimensionless)
N	Diffusional flux
n	Normal vector
n	Number of electrons transferred
q	$e^{-f\eta}$
R	Universal gas constant
r	$e^{g\theta}$
T	Absolute temperature
v	Scan rate
α	Transfer coefficient (symmetry factor)
Γ	Amount of adsorbed species per unit area
Γ_0	see Γ_{max}
Γ_{in}	Amount of adsorbed species per unit area prior to the commencement of potential sweep (known, pre-set value)
Γ_{max}	Monolayer of adsorbed species per unit area
Γ_{recov}	Amount of adsorbed species per unit area prior to the commencement of potential sweep, as determined from modelling or analysis of experimental data
$\Gamma_{Red,max}$	Monolayer of adsorbed Red per unit area
$\Delta G°_{ads}$	Standard free energy of adsorption
Δi_p	Difference in peak currents on diffusional CVs complicated and not complicated by adsorption of redox species
η	overpotential, $E - E_0$
θ	Fractional amount of adsorbed species
σ	Parameter controlling potential dependence of K

Acknowledgements

This work was supported by the European Research Council (ERC-2009-AdG 247143-QUANTIF). G.Z and A.S.C. acknowledge support by Chancellor's International Scholarships at the University of Warwick.

Notes and references

1 K. Holt, P. Hall, J. Foord, I. Kinloch and J. Macpherson, Eds., *Faraday Discussions: Carbon in Electrochemistry, vol. 172*, Cambridge, 2014.
2 W. Yang, K. R. Ratinac, S. P. Ringer, P. Thordarson, J. J. Gooding and F. Braet, *Angew. Chem. Int. Ed.*, 2010, **49**, 2114–38.
3 J. Wang, *Electroanalysis*, 2005, **17**, 7–14.

View Article Online
DOI: 10.1039/C5CP06325F

4 T. Kuila, S. Bose, P. Khanra, A. K. Mishra, N. H. Mik and J. H. Lee, *Biosens. Bioelectron.*, 2011, **26**, 4637–4648.
5 P. Huang, L. Jing, H. Zhu and X. Gao, *Acc. Chem. Res.*, 2013, **46**, 43–52.
6 L. Qu, Y. Liu, J. B. Baek and L. Dai, *ACS Nano*, 2010, **4**, 1321–1326.
7 M. Kaempgen, M. Lebert, N. Nicoloso and S. Roth, *Appl. Phys. Lett.*, 2008, **92**, 11–14.
8 R. A. Fisher, M. R. Watt and W. Jud Ready, *ECS J. Solid State Sci. Technol.* , 2013, **2** , M3170–M3177.
9 X. Xiao, T. Li, Z. Peng, H. Jin, Q. Zhong, Q. Hu, B. Yao, Q. Luo, C. Zhang, L. Gong, J. Chen, Y. Gogotsi and J. Zhou, *Nano Energy*, 2014, **6**, 1–9.
10 A. Shen, Y. Zou, Q. Wang, R. a W. Dryfe, X. Huang, S. Dou, L. Dai and S. Wang, *Angew. Chem. Int. Ed.*, 2014, 10804–10808.
11 J. C. Byers, A. G. Güell and P. R. Unwin, *J. Am. Chem. Soc.*, 2014, **136**, 11252–11255.
12 A. G. Güell, K. E. Meadows, P. V. Dudin, N. Ebejer, J. C. Byers, J. V. Macpherson and P. R. Unwin, *Faraday Discuss.*, 2014, **44**, 439–455.
13 A. N. Patel, S. Tan, T. S. Miller, J. V Macpherson and P. R. Unwin, *Anal. Chem.*, 2013, **85**, 11755–11764.
14 G. Zhang, A. S. Cuharuc, A. G. Güell and P. R. Unwin, *Phys. Chem. Chem. Phys.*, 2015, **17**, 11827–11838.
15 A. N. Patel, M. G. Collignon, M. A. O'Connell, W. O. Y. Hung, K. McKelvey, J. V Macpherson and P. R. Unwin, *J. Am. Chem. Soc.*, 2012, **134**, 20117–20130.
16 S. C. S. Lai, A. N. Patel, K. McKelvey and P. R. Unwin, *Angew. Chem. Int. Ed.*, 2012, **51**, 5405–5408.
17 P. Allongue, M. Delamar, B. Desbat, O. Fagebaume, R. Hitmi, J. Pinson and J. Savéant, *J. Am. Chem. Soc.*, 1997, **119**, 201–207.
18 P. M. Kirkman, A. G. Güell, A. S. Cuharuc and P. R. Unwin, *J. Am. Chem. Soc.*, 2014, **136**, 36–39.
19 P. Sun and M. V Mirkin, *Anal. Chem.*, 2006, **78**, 6526–6534.
20 J. Velmurugan, P. Sun and M. V Mirkin, *J. Phys. Chem. C*, 2009, **113**, 459–464.
21 J. F. Smalley, S. W. Feldberg, C. E. D. Chidsey, M. R. Linford, M. D. Newton and Y.-P. Liu, *J. Phys. Chem.*, 1995, **99**, 13141–13149.
22 A. G. Güell, N. Ebejer, M. E. Snowden, J. V. Macpherson and P. R. Unwin, *J. Am. Chem. Soc.*, 2012.
23 A. G. Guell, A. S. Cuharuc, Y. Kim, G. Zhang, S. Tan, N. Ebejer and P. R. Unwin, *ASC Nano*, 2015, **9**, 3558–3571.
24 A. J. Wain, A. J. Pollard and C. Richter, *Anal. Chem.*, 2014, **86**, 5143–5149.
25 I. Dumitrescu, P. R. Unwin, N. R. Wilson and J. V. Macpherson, *Anal. Chem.*, 2008, **80**, 3598–3605.
26 A. G. Güell, N. Ebejer, M. E. Snowden, K. McKelvey, J. V. Macpherson and P. R. Unwin, *Proc. Natl. Acad. Sci.*, 2012, **109**, 11487–11492.
27 P. Bertoncello, J. P. Edgeworth, J. V. Macpherson and P. R. Unwin, *J. Am. Chem. Soc.*, 2007, **129**, 10982–10983.
28 A. G. Güell, K. E. Meadows, P. V. Dudin, N. Ebejer, J. V. Macpherson and P. R. Unwin, *Nano Lett.*, 2014, **14**, 220–224.
29 I. Heller, J. Kong, H. A. Heering, K. A. Williams, S. G. Lemay and C. Dekker, *Nano Lett.*, 2005, **5**, 137–142.
30 A. V. Patil, A. F. Beker, F. G. M. Wiertz, H. A. Heering, G. Coslovich, R. Vlijm and T. H. Oosterkamp, *Nanoscale*, 2010, **2**, 734–738.
31 W. Li, C. Tan, M. A. Lowe, H. D. Abruña and D. C. Ralph, *ACS Nano*, 2011, **5**, 2264–2270.
32 C. Tan, J. Rodríguez-López, J. J. Parks, N. L. Ritzert, D. C. Ralph and H. D. Abruña, *ACS Nano*, 2012, **6**, 3070–3079.
33 J.-H. Zhong, J. Zhang, X. Jin, J.-Y. Liu, Q. Li, M.-H. Li, W. Cai, D.-Y. Wu, D. Zhan and B. Ren, *J. Am. Chem. Soc.*, 2014, **136**, 16609–16617.
34 N. L. Ritzert, J. Rodríguez-López, C. Tan and H. D. Abruña, *Langmuir*, 2013, **29**, 1683-1694.
35 K. K. Cline, M. T. Mcdermott and R. L. Mccreery, *J. Phys. Chem.*, 1994, **98**, 5314–5319.
36 N. Nioradze, R. Chen, N. Kurapati, A. Khvataeva-Domanov, S. Mabic and S. Amemiya, *Anal. Chem.*, 2015, **87**, 4836–4843.
37 M. Tang, K. Miyazaki, T. Abe and J. Newman, *J. Electrochem. Soc.* , 2012, **159** , A634–A641.
38 A. M. Bond, E. A. Mclennan, R. S. Stojanovic and F. G. Thomas, *Anal. Chem.*, 1987, **2860**, 2853–2860.
39 D. Mampallil, K. Mathwig, S. Kang and S. G. Lemay, *J. Phys. Chem. Lett.*, 2014, **5**, 636–640.
40 M. A. G. Zevenbergen, P. S. Singh, E. D. Goluch, B. L. Wolfrum and S. G. Lemay, *Nano Lett.*, 2011, **11**, 2881–2886.
41 S. G. Lemay, D. M. van den Broek, A. J. Storm, D. Krapf, R. M. M. Smeets, H. A. Heering and C. Dekker, *Anal. Chem.*, 2005, **77**, 1911–1915.
42 G. Zhang, P. M. Kirkman, A. N. Patel, A. S. Cuharuc, K. Mckelvey and P. R. Unwin, *J. Am. Chem. Soc.*, 2014, **136**, 11444–11451.
43 R. J. Rice and R. L. McCreery, *Anal. Chem.*, 1989, **61**, 1637–41.
44 R. Bowling, R. T. Packard and R. L. McCreery, *Langmuir*, 1989, **5**, 683–688.
45 R. J. Bowling, R. T. Packard and R. L. McCreery, *J. Am. Chem. Soc.*, 1989, **111**, 1217–1223.
46 K. R. Kneten and R. L. McCreery, *Anal. Chem.*, 1992, **64**, 2518–2524.
47 M. T. McDermott, K. Kneten and R. L. McCreery, *J. Phys. Chem.*, 1992, **96**, 3124–3130.
48 M. T. McDermott and R. L. McCreery, *Langmuir*, 1994, **10**, 4307–4314.
49 A. N. Patel, S. Tan and P. R. Unwin, *Chem. Commun.*, 2013, **49**, 8776–8778.
50 R. H. Wopschall and I. Shain, *Anal. Chem.*, 1967, **39**, 1514–1527.
51 C. M. A. Brett and A. M. Brett, *Electrochemistry: principles, methods, applications*, Oxford University Press, New York, 1993.
52 P. W. Atkins, *Physical Chemistry*, Oxford University Press, Oxford, 4th edn., 1994.
53 R. Lide, *CRC handbook of chemistry and physcis*, CRC Press, USA, 2001.
54 W. Schmickler and E. Santos, *Interfacial electrochemistry*, Springer, New York, 2nd edn., 2010.
55 Wolfram Research Inc., *Mathematica*, Wolfram Research, Inc., Champaign, Illinios, 10.0 edn., 2015.
56 M. S. Freund and A. Brajter-Toth, *J. Phys. Chem.*, 1992, **96**, 9400–9406.
57 D. Welipitiya, P. A. Dowben, J. Zhang, W. W. Pai and J. F. Wendelken, *Surf. Sci.*, 1996, **367**, 20–32.
58 J. M. Jin, W. F. Lin and P. A. Christensen, *Phys. Chem. Chem. Phys.*, 2008, **10**, 3774–3783.
59 K. Kunimatsu, M. G. Samant, H. Seki and M. R. Philpott, *J. Electroanal. Chem. Interfacial Electrochem.*, 1988, **243**, 203–208.
60 C. G. Williams, M. A. Edwards, A. L. Colley, J. V. Macpherson and P. R. Unwin, *Anal. Chem.*, 2009, **81**, 2486–2495.
61 A. Kozbial, Z. Li, J. Sun, X. Gong, F. Zhou, Y. Wang, H. Xu, H. Liu and L. Li, *Carbon*, 2014, **74**, 218–225.
62 D. Martinez-Martin, R. Longuinhos, J. G. Izquierdo, A. Marele, S. S. Alexandre, M. Jaafar, J. M. Gómez-Rodríguez, L. Bañares, J. M. Soler and J. Gomez-Herrero, *Carbon*, 2013, **61**, 33–39.
63 A. J. Bard and L. R. Faulkner, *Electrochemical Methods: Fundamentals and Applications*, John Wiley&Sons, Inc., New York, 2nd ed., 2001.

View Article Online
DOI: 10.1039/C5CP06325F

64 E. I. Sirotkina, A. N. Nesmeyanov and N. A. Vol'kenau, *Izv. Akad. Nauk SSSR, Seriya Khimicheskaya*, 1969, **7**, 1605–1606.
65 H. Gerischer and R. McIntyre, *J. Phys. Chem.*, 1987, **91**, 1930–1935.
66 S. Lhenry, Y. R. Leroux and P. Hapiot, *Anal. Chem.*, 2012, **84**, 7518–7524.

View Article Online
DOI: 10.1039/C5CP06325F

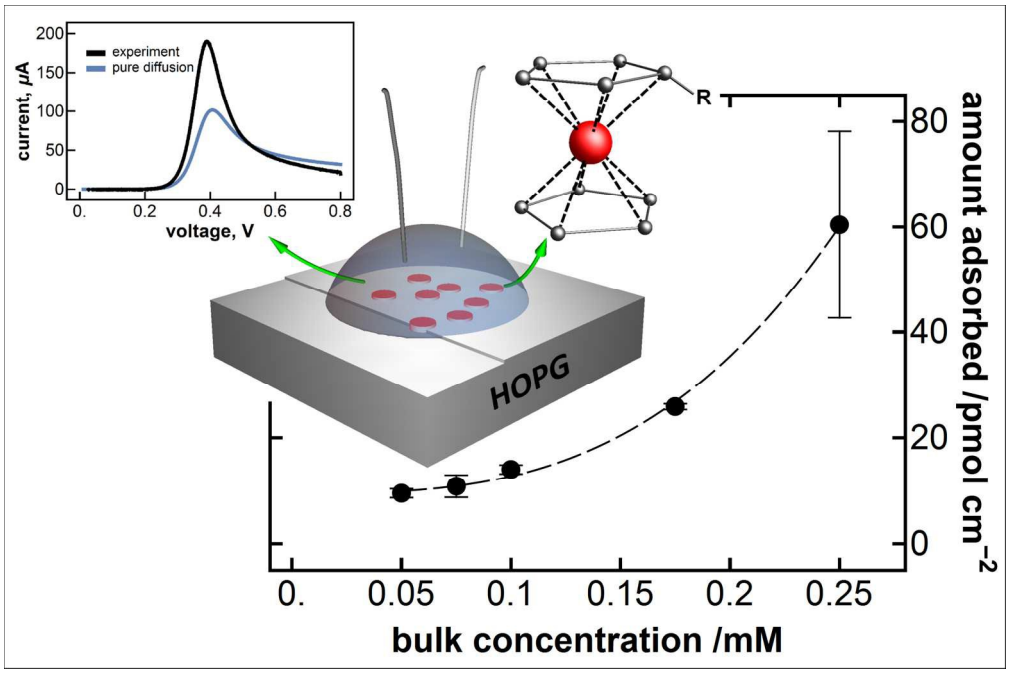

355x236mm (150 x 150 DPI)